Advanced DSP-Based Monitoring for Spatially Resolved and Wavelength-Dependent Amplifier Gain Estimation and Fault Location in C+L-Band Systems

Matheus Sena , Pratim Hazarika , Caio Santos , Bruno Correia , Robert Emmerich , Behnam Shariati , Antonio Napoli , Vittorio Curri , Wladek Forysiak , Colja Schubert, Johannes K. Fischer , and Ronald Freund

(Top-Scored Paper)

Abstract—The development of efficient anomaly detection schemes is a key element for the implementation of autonomous optical networks as they can help telecom operators to automate the location of defective devices and track the overall performance of the network infrastructure. In that regard, the exploitation of receiver based digital signal processing (DSP) for optical performance monitoring has shown to be a promising enabler for detection of spatially resolved and wavelength-dependent properties and anomalies in optical fiber links. In this work, we study the benefits of applying DSP-based longitudinal power estimation on multiple wavelength division multiplexing (WDM) channels allocated in the optical grid to infer wavelength-wise characteristics of a C+L-band optical line system. In that context, we show that the applied scheme can successfully recreate a visualization of the spatial evolution of the gain tilt imposed by in-line optical amplifiers. Additionally, we propose the utilization of advanced DSP tools based on wavelet-denoising to enhance the performance of an anomaly detection approach. The proposed method not only can improve accuracy of the fault location, by reducing positioning uncertainty, but it also delivers more uniform readings of the anomaly signatures.

Index Terms—Anomaly detection, C+L-band, digital signal processing, fiber nonlinearity, optical performance monitoring.

I. INTRODUCTION

A RELIABLE migration from current C-band to a multi-band (MB) optical network [1] will also depend on the development of monitoring mechanisms that are able to deliver low-cost but accurate estimation of wavelength-dependent and spatially resolved properties of optical devices (e.g., amplifiers [2], [3] switches [4], [5], and transceivers [6]). In that context, receiver (Rx) based digital signal processing (DSP) methods have been extensively explored to estimate properties of optical fiber links [7], [8], [9], [10], [11], [12], [13], [14], [15], [16], [17], thus relaxing the demanding requirements of deploying multiple and expensive node-level measurement devices. Thanks to their capability in unveiling multi-span link characteristics, such as longitudinal power evolution [7], [8], [9], [10], [11], [12], frequency response of optical filters [12], chromatic dispersion mapping [13], Raman gain [14], and polarization-dependent loss [15], these Rx-DSP monitoring methods have gained a momentum over the past few years.

One successful example of Rx-DSP for estimation of link properties was demonstrated in [8], the so-called in-situ power profile estimator (PPE). This method reconstructs the channel power profile along an optical link, which consequently enables the prediction of anomalous attenuation points with sub-km resolutions [9]. In our previous contribution, i.e., [16], we showed that by applying the in-situ PPE on multiple wavelengths of a C+L-band transmission system, it is possible to create a distance-wise, wavelength-dependent link tomography. This is a simple 3D-visualization of the relation power versus wavelength versus distance and helps to reveal MB characteristics of the deployed in-line optical amplifiers, e.g., spectral gain. In [16], it was also shown that the link tomography can directly support the identification of failures such as anomalous gain tilt imposed by malfunctioning amplifiers. Recently, our work published in

[17] also successfully demonstrated that another type of amplification fault, i.e., the narrowband gain compression caused by the spectral hole-burning (SHB) effect, can be likewise captured by using the link tomography.

Despite all credits that [16] and [17] deserve, the experimental results presented in these contributions comprise a methodology where a single wavelength-division multiplexing (WDM) channel is swept across the wavelength domain in order to capture the frequency-dependent information of the optical system. This methodology, consequently, is subject to at least two important implications. First, it is not suitable for running/operational WDM systems, since a "probe" channel cannot be deliberately tested on multiple wavelengths without switching off active services. Second, this single-channel analysis is immune to the interference originated from adjacent carriers, i.e., cross-channel interference. Therefore, we believe that a C+L-band multi-channel analysis is an interesting and more realistic study that would finally complement the discussions present in [16] and [17].

Another important topic discussed in [17] is the development of fault detection schemes that can further improve the identification of anomaly signatures. As efficient anomaly detection schemes are of key importance for network operators, helping them to carry out more assertive maintenance routines, we believe that the proposal of a novel scheme, with improved performance compared to the one shown in [17], is another appropriate subject for extension in this paper.

In this work, we experimentally investigate a Rx-DSP based link tomography to estimate spectral gain, visualize tilt evolution and detect anomalies generated by Erbium-doped fiber amplifiers (EDFA)s in a C+L-band transmission setup. The results reported in this manuscript complement our previous discussions initiated in [16] and [17] in three different aspects, which are listed below.

1) *Technical details:* Underlying explanations on how to obtain spectral gain of EDFAs and that support the results presented in [16] are described with more details.

2) *Novel multi-channel experimental analysis:* Opposed to [16] and [17], where a single-channel methodology was carried out, this work introduces a new experimental campaign based on a multi-channel transmission setup. Besides being a more realistic scenario, this permits to extract information from each individual WDM channel without the necessity of a probe channel. This scheme is applied to visualize the spatial evolution of the gain tilt.

3) *Introduction of denoising tool for anomaly detection:* A denoising tool based on wavelet transformation is introduced to improve location of faults and deliver more uniform reading of the anomaly signatures.

The remainder of this text is structured as follows. Section II summarizes related works with significant synergy with the topic discussed in this text and clarifies this paper's position. Section III briefly the concept and application of link tomography. Section IV presents some additional details of the single-channel experimental results presented in [16], where the link tomography is applied to estimate amplifier spectral gain in optical links. Section V introduces the new experimental analysis obtained with the application of the link tomography in a multi-channel scenario. In that respect, we demonstrate how the link tomography can reveal the evolution of gain tilts and propose how an advanced DSP denoising technique can reduce uncertainty of fault location. Finally, Section VI draws the conclusions and considerations of this work.

II. RELATED WORK

One of the most straightforward ways to increase capacity of optical line systems (OLS)s is through the exploitation of techniques that can efficiently utilize the widely available spectrum in optical fibers [1]. In that respect, upgrading conventional C-band WDM systems to C+L-band becomes the most obvious and short-term move towards a cost-effective expansion of capacity in optical fiber networks. On the other hand, designing, deploying and operating such systems is a more challenging task in comparison to today's C-band-based operation. To overcome this obstacle, ongoing research has heavily focused on multiple aspects to drive a fast deployment of C+L-band transmission systems. Two important aspects that are worth mentioning are: (1) amplification technologies, and (2) launch power strategies. With respect to (1), commercially available EDFAs [18] or hybrid Raman/EDFA amplification have shown promising performance in C+L-band, with the latter presenting breakthroughs of 56.4 Tb/s over 800 km of fiber [19]. Concerning (2), launch power optimization approaches aim at counteracting the quality of transmission (QoT) degradation mainly caused by stimulated Raman scattering (SRS) [20]. In that regard, several works have shown that non-flat input power profile can compensate for the SRS effect, being able to deliver a considerable high and flat QoT over the entire C+L-band WDM grid [21], [22], [23].

In order to support these two aspects, i.e., deployment of novel MB amplification technologies and application of launch power strategies in C+L-band systems, optical networks will require powerful wavelength- and distance-wise monitoring mechanisms. These mechanisms will facilitate launch power management of MB EDFAs and permit us to keep track of aging and malfunctioning processes in these novel MB technologies. Nonetheless, to guarantee precise optical performance monitoring (OPM), network operators usually face the business-limiting aspects imposed by node-level monitoring approaches, i.e., when multiple measurement devices are allocated across complex and nationwide networks. This, however, can be relaxed with the development of terminal-based OPMs, which solely exploit the Rx-DSP modules to estimate properties of optical fiber links. Such a solution stands out as a competitive alternative over node-level monitoring, given that data from in-line devices could be directly streamed out from the transceivers rather than from dedicated measurement devices.

Recently, several link properties, such as longitudinal power evolution [7], [8], [9], [10], [11], [12], frequency response of bandpass filters [12], span-wise chromatic dispersion mapping [13], Raman gain [14], and polarization-dependent loss profile [15] have been obtained through Rx-DSP. In general terms, the basic principle that permits the extraction of these physical properties is the fact that the optical link can be analytically
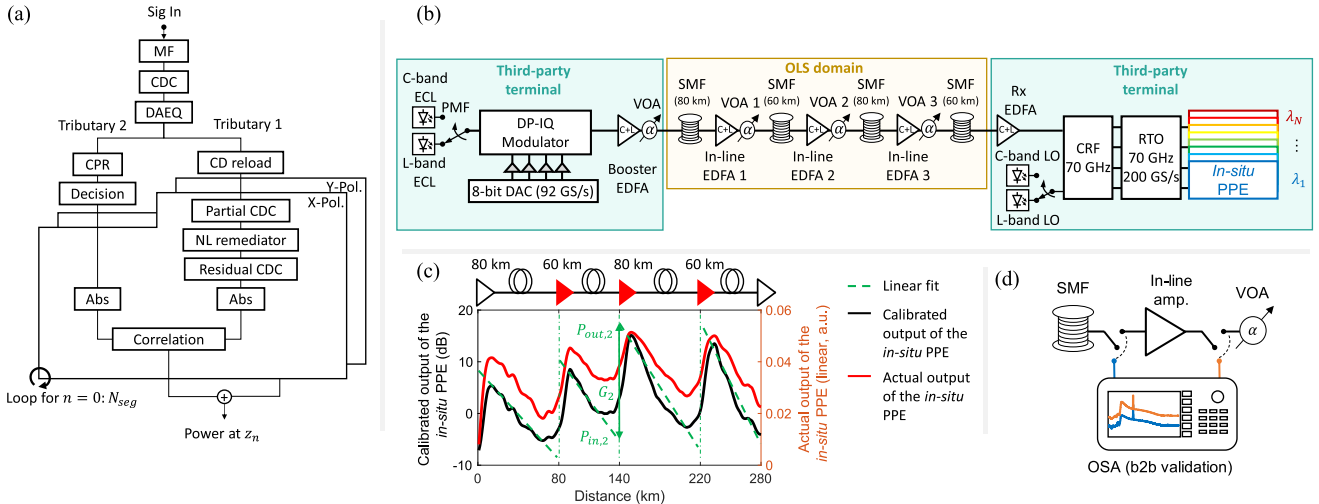
Fig. 1. (a) Block diagram of the in-situ PPE algorithm used in this paper. (b) Setup utilized in the Experiment I, where a single-channel analysis is performed to obtain the gain profile of the in-line EDFAs 1, 2 and 3. (c) Method to estimate the gain of the i-th in-line amplifier (G_i) at a fixed wavelength. (d) Scheme utilized in the b2b validation of the amplifier gain profile. Abs: Absolute value of the signal samples. CD: Chromatic dispersion. CDC: Chromatic dispersion compensation. CPR: Carrier phase recovery. DAEQ: Data-aided adaptive equalizer. MF: Matched filter. PMF: Polarization maintaining fiber.

modeled using conventional split-step Fourier method. Then, the parameters of this model are recursively estimated once a replica of the transmitted information (obtained from the Rx-DSP chain) is compared against the signal recovered through digital backpropagation (DBP) [24].

In the work presented in [8], for instance, a low-complexity and simplified DBP algorithm was proposed, which permits the visualization of the longitudinal power profile in multi-span fiber links. This algorithm, named in-situ PPE, can be consequently used in the construction of a link tomography, which corresponds to a spatially and wavelength-resolved visualization of power evolution [16]. The link tomography may then assist (in the short-term) the implementation of MB systems as power-related, wavelength-dependent physical properties of fiber links can be estimated at a lower cost relative to traditional monitoring approaches.

Although the present work has some correspondences with the above-cited references, especially, [7], [10], [14], [17], we believe that the new investigations emphasized in this manuscript make it self-standing and for the following reasons.

Firstly, despite the technique used to create the link tomography in this paper is the in-situ PPE, broadly discussed in [7], in their contribution the authors solely apply the data from an individual channel to focus on spatially resolved characteristics of the link. In that way, the information embodied in the wavelength domain is not exploited, as opposed to what we propose. This clearly distinguishes this present paper from [7].

In [10] and [14], contrarily to [7], both the spatial and wavelength domains are explored to reveal the gain of hybrid Raman/EDFAs. However, while the authors in [10] and [14] adopt a single-channel methodology (similar [17]) for C-band-only systems, our experimental campaign englobes both C-and L-band in a multi-channel transmission scenario, which resembles with more fidelity the conditions of an operational network. Finally, the investigations in [10] and [14] focus on the

DSP for estimation of amplifier gain, whereas ours approaches both gain estimation and detection of anomalies. Concerning the anomaly detection, our work even proposes a novel method to improve the identification of amplification faults, thus extending the discussions shown in [17].

III. BACKGROUND

The link tomography proposed in this work is based on the in-situ PPE devised by T. Tanimura et al. in [8]. However, we would like to point out that other powerful approaches, such as the one extensively studied in [10], [11], [12], [13], [14], could be analogously applied. This means that the objective of this contribution is to explore the possibilities that these DSP-based monitors can offer rather than to draw any performance comparison among approaches. That being said, the fundamental idea of the in-situ algorithm is to provide a monitor that delivers a per-channel longitudinal power profile along an optical fiber link. Because the in-situ PPE was already broadly described in [7], [8], [9], [17], in this text we simply summarize it in in the block diagram shown in Fig. 1(a) and provide a very short explanation about its core idea and some parameter configuration used in the algorithm.

Briefly, the core idea proposed by the authors in [8] is to apply basic DSP functions on two signal tributaries (Tributary 1 and 2 in Fig. 1(a)) and, in the sequence, calculate the correlation between these processed signals to estimate a quantitative indicator of power at a distance z_n (from the receiver side). Then, the algorithm is run within a loop that calculates this correlation for multiple link segments, represented by the index n, which varies from 0 to N_{seg}. This permits the spatial reconstruction of the power profile along the entire link. Consequently, when the in-situ PPE is applied to multiple WDM channels ($\lambda_1 - \lambda_N$), as illustrated for the OLS in Fig. 1(b), it is possible to build a wavelength-resolved and distance-wise visualization

of the power evolution along an optical link. This visualization was denominated in [16] as link tomography and can be considered as a first step towards the design of a networkwide tomography [7].

In order to calculate the correlation between Tributary 1 and 2, we have used data processing blocks of 2^{15} samples (32768 samples), which is a longer window than the 2^{11} samples used in [9]. Although this makes the algorithm slower, given the higher number of samples to be processed, we noticed that, in turn, a reduced number of averagings could be applied to achieve a rather smooth longitudinal power estimation curve. Therefore, in the first experimental analysis presented in this work (single-channel study) we nominally applied 8 averagings to the output of the in-situ PPE for all wavelengths, with exception of 1562.5 and 1565 nm, where 10 averagings were performed, due to the lower gain regime and higher noise susceptibility in this spectral region. In the second experiment (multi-channel), we nominally applied 10 averagings to all wavelengths. Of course, we know that further improvements could be eventually achieved if the averaging window is increased, which is something left to be investigated in the future. For this work, as our analysis involved multiple wavelengths, we attempted to find a compromise between an acceptable accuracy and the processing complexity when building the link tomography.

The output of the in-situ PPE, as pointed out earlier in the text, provides "a quantitative indicator of the signal power at a distance z_n." In order to map this quantitative indicator to the true optical power in linear scale, an affine transformation (calibration) is necessary [25]. This is important because in the first part of this paper we use the link tomography to estimate the spectral gain of the individual in-line EDFAs. The first step of the calibration process consists of progressively attenuating the output of the amplifier under test (AUT) and comparing the peak values estimated from the in-situ PPE (in a.u.), saved in the vector $\mathbf{P}_{est}$, with the actual measurement from an optical spectrum analyzer (in mW), saved in the vector $\mathbf{P}_{OSA}$. Measuring the peak power values of the AUT is strategic, as this is the point (in the spatial domain), with the highest self-phase modulation (SPM), which contributes to a more accurate estimation of the in-situ PPE output, in comparison to other points in the middle or at the end of the span. Then, with both of these vectors, namely, $\mathbf{P}_{est}$ and $\mathbf{P}_{OSA}$, we perform a linear regression to find the scaling coefficient (α) and the offset (β) that optimally map $\mathbf{P}_{est}$ into $\mathbf{P}_{OSA}$, i.e., that minimize the expectation $E[\|\mathbf{P}_{OSA} - \alpha\mathbf{P}_{est} - \beta\|^2]$. In this way, one can obtain a calibrated output $P_{cal} = \alpha P_{est} + \beta$, where P_{est} is any point-wise value of the output of the in-situ PPE. In order to be consistent, this operation was repeated for all wavelengths such that an averaged scaling factor $\bar{\alpha}$ and offset parameter $\bar{\beta}$ could be used in our analysis. Although this calibration was performed with the direct utilization of an optical spectrum analyzer (OSA) on the link under test, we believe that the inference of the parameters α and β can be carried out beforehand. For instance, simulative analysis or tests on pre-built lab experimental setups can be run to estimate α and β. Evidently, the calibration parameters can significantly vary depending on the transmission scenario (e.g., channel power, number of channels, symbol rate),

causing a more severe or moderate spread of waveforms, which leads to higher or lower correlation values. One interesting solution that would facilitate the practical implementation of this approach is the use of look-up tables that could suggest values for the calibration parameters based on different transmission configurations.

It is important to highlight that only few essential link parameters are necessary to infer the longitudinal power evolution. Firstly, the total link length, which is then used as a reference for the spatial resolution of the algorithm. Secondly, the accumulated chromatic dispersion (CD) at the receiver, as it must be loaded to the tributary 1, according to the diagram shown in Fig. 1(a). However, with the aid of modern DSP modules, CD can be easily estimated without much knowledge of the dispersion mapping of the link. At last, in case CD pre-distortion is applied on the transmitter side, this value must be also known a priori and discounted from the accumulated CD at the receiver side.

One of the main parameters of the in-situ PPE is the ε, which is a nonlinear remediation coefficient [9]. Physically speaking, it serves the purpose to coarsely equalize a nonlinear distortion on top of the optical waveform at the point in space corresponding to the index n. For the purpose of visualization of the longitudinal power profile, the authors in [9] suggest setting ε to a low value, i.e., 0.01. In our studies, we tested a few values for ε in the vicinity of 0.01 and visually noticed a slightly smoother profile for the longitudinal power estimation by setting ε to 0.004, which was then used throughout this work.

IV. DISCUSSION

A. Experiment I

In the first experiment discussed in this work, we demonstrate how the link tomography can be used to extract the gain of optical amplifiers. For that, we kindly ask the reader to inspect the diagram depicted in Fig. 1(b). As shown in the illustration, the transmitter consists of a 4-ch 92 GSa/s DACs (operated at 84 GSa/s) and a standard C-band optical multi-format transmitter composed of a set of four driver amplifiers and a LiNbO3-based dual-polarization (DP) IQ-modulator. To compensate for undesired MB impairments induced by the transmitter components, Volterra-based digital pre-distortion (DPD) was employed as it has been proven to successfully suppress transmitter (non)linear distortions in S+C+L-band systems [26]. For the Volterra DPD, we used a truncated, time-invariant 3rd-order Volterra filter with 256 taps in the first order, and 9 taps in the second and third orders. In the sequence, this DPD filter is applied on a 64-GBd DP-16-QAM signal generated with a 2^{15} pseudo-random bit sequence and shaped with a root-raised cosine pulse filter (roll-off factor 0.1). In addition to the DPD, a chromatic dispersion pre-compensation of 800 ps/nm was also performed on the transmitter side and added to the signal, as suggested in [8].

Since a single-channel investigation was carried out in this first experiment, to emulate the multiple WDM channels, two tunable external cavity laser (ECL, <100 kHz linewidth) sources have been used individually for generation of the tested carriers in the C- (1527.5–1565 nm), and in the L-band (1570–1600 nm). Then, the central wavelength of the ECLs was varied in steps
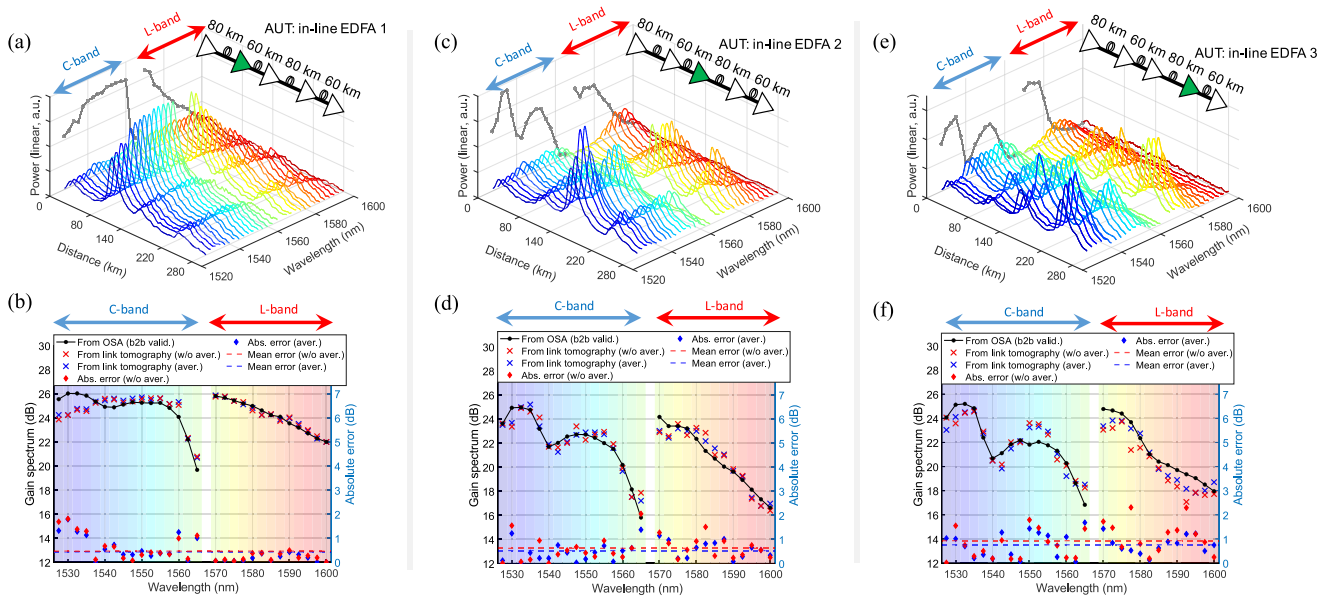
Fig. 2. Link tomography for the estimation of the spectral gain profile (at constant input power of - 8 dBm), when the AUT is the in-line EDFA (a) 1, (c) 2 and (e) 3. In (a), (c), and (e), the power peaks estimated by the link tomography of the in-line EDFA 1, 2 and 3, respectively, are projected onto the background plane parallel to the wavelength axis. Comparison between gain spectrum obtained from OSA and from link tomography for the in-line EDFA (b) 1, (d) 2 and (f) 3. Results obtained for $N_{seg} = 280$ and $\varepsilon = 0.004$.

of 2.5 nm while maintaining a constant input power into the modulator of 16 dBm. In this way, the channel under test (CUT) could be swept across the investigated spectrum and the in-situ PPE run for all tested wavelengths.

The OLS under investigation consisted of two 80-km fiber spools, deployed in the 1st and 3rd span, and other two 60-km spools, deployed in the 2nd and 4th spans. As for the EDFAs, all units, including terminal and in-line amplifiers, were configured to operate for $1540 - 1565$ nm (C-band) and $1570 - 1605$ nm (L-band). The EDFAs were also programmed in automatic current control (ACC) mode, where maximum pump currents of either 350 mA, in the C-band, or 700 mA, in the L-band, were supplied.

After signal reception by a coherent receiver frontend (CRF, 70 GHz of bandwidth), a 200 GSa/s RTO (70 GHz of elecrical bandwidth, 8-bit resolution) was used to sample the analog electrical signal and to deliver the digitized signal to the Rx-DSP chain, in charge of the longitudinal power estimation and depicted in the block diagram in Fig. 1(a). For the DAEQ, we used a memory length of 61 taps.

B. Gain Estimation

The first application derived from the link tomography concerns the estimation of spectral gain of the in-line amplifiers. As mentioned early in the text, the spectral gain estimation is only possible thanks to the power profile provided by the link tomography. To better illustrate it, we provide an example in Fig. 1(c), which depicts both, the calibrated and the actual outputs of the in-situ PPE for an arbitrary wavelength. As it can be seen, the input ($P_{in,2}$) and output ($P_{out,2}$) power of the 2nd in-line EDFA (at the 140th km) can be extracted from the calibrated curve. Therefore, the difference between these two

values (in dB) embodies the gain of the amplifier, here denoted by G_2. As a mean to improve the estimations of G_i (gain of the i-th in-line EDFA), a simple linear fit (Fig. 1(c)) can be also applied on the monotonically decreasing portion of the power profile curve, such to minimize the mean squared error between the fit and the span-wise power profile. In order to validate this methodology, the gain obtained from the link tomography is benchmarked against the back-to-back (b2b) extraction depicted by the schematic in Fig. 1(d), where an optical spectrum analyzer (OSA) is utilized to measure the input and output power at each AUT and directly obtain the corresponding OSA gain. When estimating the gain profile through both methods, i.e., via link tomography and b2b validation, the input power of the AUT is maintained at a constant value of -8 dBm.

We emphasize that in this experimental investigation, variable optical attenuators (VOA)s were added to the output of the EDFAs, thus avoiding very high input power into the fiber spans that could complicate the recovery of the reference signal in the tributary 1 DSP chain. Therefore, the link tomography always delivers the resulting power of the two equipment, i.e., EDFA + VOA, as they virtually act as a single device. In this way, we correct the amplifier gain from the link tomography by numerically adding the attenuation of the VOA, which is known *a priori*.

In the way we carried out this single-channel experiment, we tried to maintain the link launch power at approximately 8 dBm by controlling the VOA after the booster EDFA. This was necessary because the link tomography becomes very efficient for high SPM regimes, i.e., high launch power. However, given that the in-line EDFAs 1, 2 and 3 were programmed to run in the ACC mode, which means that their gain varies such that the provided current is maintained constant, the launch power of

each span was not fixed, but rather changed with the investigated wavelength.

The results in Fig. 2(a), (c), (e) show the link tomography (direct output of the in-situ PPE) for the AUT 1, 2 and 3, respectively. The color-coding from dark blue to dark red correspond to the longitudinal power profile extracted from the WDM channel at each tested wavelength in the C- and L-band. As can be noted, the presence of four significant spikes along the distance axis correlate with the power rise provoked by the Booster EDFA and in-line EDFAs 1, 2 and 3. For the purpose of illustration, let us now concentrate on the results from the characterization of the AUT 2, which can be further generalized to the other amplifiers. In Fig. 2(c), we plot on the background plane the power peak (grey solid dot-like markers) that the channel experiences when propagating through AUT 2 (around 140 km). In the C-band, for example, the AUT 2 manifests a very strong gain at ∼1535 nm, which is followed by a lower-gain profile with a parabolic-like shape from 1542.5 nm to 1565 nm. As for the L-band, the AUT 2 has a significant tilt profile with reduced gain as the channel central wavelength approaches 1600 nm.

In Fig. 2(d), it is possible to visualize the gain profile curve obtained from the b2b validation of the AUT 2, which is denoted by the black solid dot-like markers. As expected, this gain profile follows the same nature of the power peaks caused by the AUT 2, indicated in Fig. 2(c) (grey dot-like markers). Now, a direct comparison between the b2b validation and the gain extracted from the link tomography (blue cross-like markers in Fig. 2(d)) confirms the good agreement between both approaches. This agreement can be also quantified in terms of an absolute error between both methodologies, which is depicted by the blue diamond-like markers in Fig. 2(d). It is also observable that the mean error value over all wavelengths (blue dashed line) reaches approximately 0.5 dB. In Fig. 2(d), it is possible to observe the result of the spectral gain estimation when no averaging is applied to the link tomography (red cross-like markers), which leads to a slightly higher mean error (red dashed line) than the averaged case.

Although the previously mentioned results concern the characterization of the AUT 2, an identical analysis can be drawn for AUT 1 (Fig. 2(a), (b)) and AUT 3 (Fig. 2(e), (f)). In summary, we find out that the agreement between both gain extraction methodologies, i.e., via b2b validation and via link tomography, remains consistent as an error of nearly 0.4 and 0.6 dB (blue dashed line) can be achieved for AUT 1 (Fig. 2(b)) and AUT 3 (Fig. 2(f)), respectively.

Finally, it is noteworthy mentioning that this single-channel methodology for gain estimation can be a suitable tool in greenfield applications as the CUT is freely swept over the spectrum without interrupting the network operation.

C. Experiment II

The gain estimation results from Experiment I represent one of the main contributions of our work presented in [16]. In this second experiment, our goal now is to focus on anomaly detection. Additionally, we investigate the link tomography in a more realistic WDM transmission scenario than the one studied so far.

In this new testbed (Fig. 3), interfering channels are generated by shaping amplified spontaneous emission noise through wavelength selective switches (WSS)s. Subsequently, the generated channels are fed to C- and L-band Booster EDFAs, then multiplexed with a 3-dB coupler and finally combined with the CUT, which was analogously generated according to the description already introduced in section IV.1. In total, 42 channels, i.e., 20 channels in C-band and 22 channels in L-band, were launched into the fiber with a spectrally flat power profile (total launch power of 14.9 dBm), which implies that no launch power optimization was performed. Additionally, all interfering channels presented the same bandwidth as the CUT and were equally spaced by approximately 1.18 nm (∼150 GHz channel spacing). We do expect that narrower channel spacing can lead to a significant performance degradation. This occurs due to a stronger influence of the cross-phase modulation (XPM), which dramatically increases as the channels become more densely packed. Therefore, we foresee that the application of such a link tomography should initially target partially loaded links. Between C- and L-band, we created a gap band of 13.52 nm (∼ 1.645 THz).

At the receiver side, the optical power of the WDM grid is boosted by an EDFA before being filtered through a bandpass filter (BPF) for the selection of the CUT. The signal before the filter is also used for optical signal-to-noise ratio measurements through an OSA. The selected channel is then amplified one last time before being mixed with the local oscillator (LO) at the coherent receiver.

In this new experiment, the central wavelength of the CUT was swept from 1537.83 nm to 1600.50 nm, with steps of 2.36 nm, i.e., skipping every other channel. In that way, the WSSs were accordingly programmed to account for the insertion of the CUT when the in-situ PPE was running at a specific wavelength. We highlight that this sweeping process was needed due to the absence of additional optical transmitters. In a real-world scenario, the wavelength-based information should be extracted from each deployed channel.

D. Multi-Channel Power Visualization

Before exploring the anomaly detection schemes, let us first inspect some additional outcomes that can be directly extracted from the link tomography (Fig. 4(a)) and may also serve as indicators about the health of the transmission system.

Similarly to the results shown in Fig. 2(a), (c), (e), the color-coded curves (from dark blue to dark red) in Fig. 4(a) correspond to the longitudinal power profile extracted from the WDM channel at each tested wavelength in the C- and L-band. It is important to mention that unlike the results in Fig. 2(a), (c), (e), where each link tomography is obtained such that the input of the characterized AUT is constant, in this new analysis only one link tomography is necessary. That means that the input power experienced by each individual amplifier possibly differs from one device to another. This methodology, in contrast to the one shown in Subsection IV.2, is more appropriate for brownfield
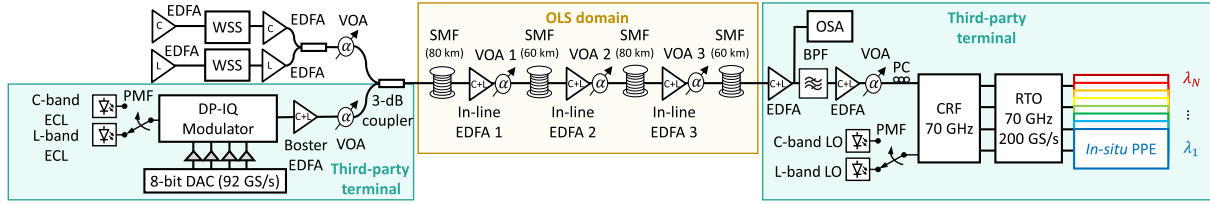
Fig. 3. Setup utilized in the Experiment II, where a multi-channel analysis is performed to detect anomalies caused by the optical amplifiers. Polarization controller (PC).
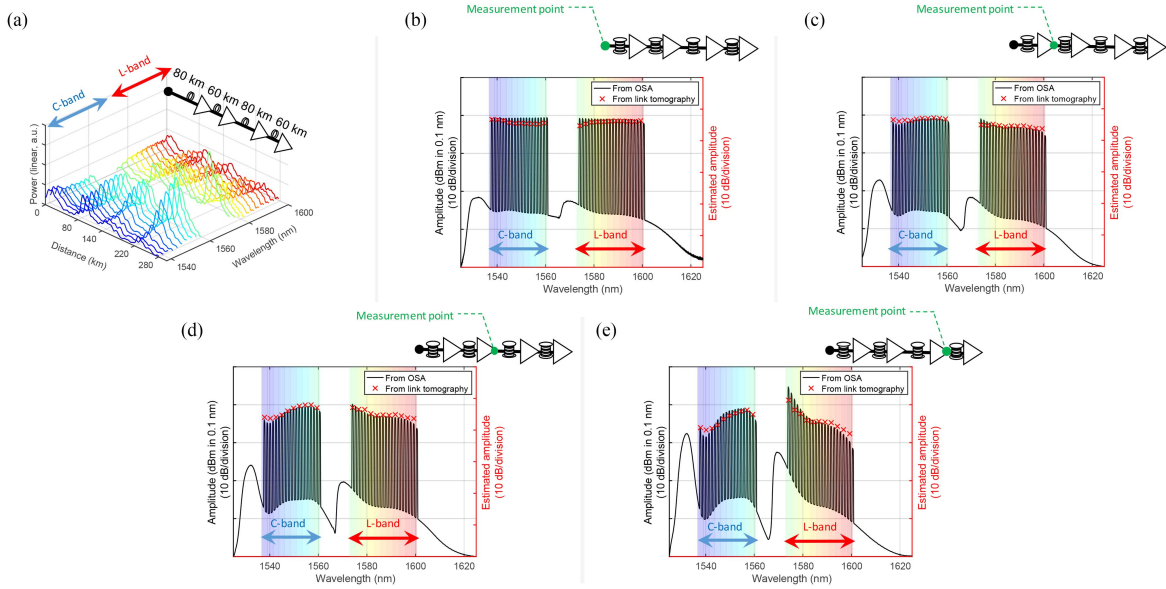

Fig. 4. (a) Link tomography obtained in Experiment II (multi-channel analysis). Power peak curves obtained from the link tomography obtained at (b) input of the OLS, and output of the in-line EDFA (c) 1, (d) 2 and (e) 3 link, when compared against spectrum from an OSA. The measurement point indicates the location in the link, where this comparison was performed. Results obtained for $N_{seg} = 280$ and $\varepsilon = 0.004$.

purposes, i.e., when the system is already in operation and adjustments in the link (e.g., setting a constant input to each amplifier) should be avoided.

The first benefit of this visualization is that it promptly indicates the gain nature due to each EDFA deployed in the link. This is visible in Fig. 4(b)–(e), where the power peaks at the input of the OLS, and at the output of the in-line EDFA 1, 2 and 3 (red cross-like markers), are contrasted against their corresponding spectra obtained from an OSA (black solid line). It is interesting to observe in these results that despite the flat power profile launched into the OLS, the gain tilt in the WDM grid evolves significantly. In the C-band, for instance, the loss evolves in the direction of the lower wavelengths, whereas in the L-band the opposite occurs, i.e., the loss increases towards higher wavelengths. This is successfully captured by the link tomography results (red cross-like markers in Fig. 4(b)–(e)), which follow an identical profile to what was predicted from the OSA measurements.

E. Tilt Detection

The tilt evolution reported in Fig. 4(b)–(e) is a natural process that usually happens in transmission systems due

to cascaded amplification. Other factors can also worsen amplification tilts, for instance, channel-loading configurations or variations in channel input power [27]. The latter, for instance may be caused by imperfect fiber-to-amplifier connectors. In order to confirm whether the link tomography can successfully capture this anomaly, we emulate an excessive attenuation at the input of in-line EDFA 2 by inserting a VOA with a spectrally flat 6-dB attenuation profile. By doing so, we expect that a gain tilt will be generated at the output of the in-line EDFA 2, since the incoming power is now 6 dB lower. Then, we apply very simple scheme to locate link failure, which is based on the direct difference between two monitored states of the link tomography, i.e., one without anomaly (reference) and one with anomaly (continuously monitored), as proposed in [8] and depicted in Fig. 5(a). The result of this subtraction is then projected on a heat map as illustrated in Fig. 5(b). As can be observed, two important anomaly "signatures" are clearly visible from the heat map. The first one, in the vicinity of 140 km, indicates the emulated tilt on the in-line EDFA 2. Given the wavelength-dependency of this signature and the proximity to the in-line EDFA 2, this anomaly is easily distinguishable from other link faults, such as excessive attenuation points in the fiber, which has a wavelength-independent profile. The second
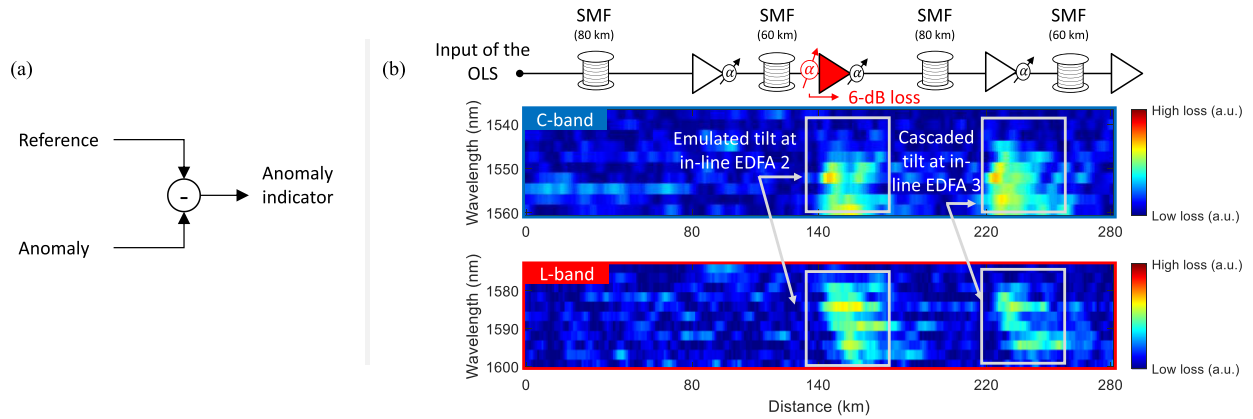
Fig. 5. (a) Anomaly detection scheme based on the subtraction of the anomalous link tomography from the reference one. (b) Anomaly indicator map based on the subtraction scheme when an additional VOA with a spectrally flat 6-dB loss profile is inserted at the input of in-line EDFA 2. The change of the input power causes a tilt at in-line EDFA 2 and a cascaded effect at in-line EDFA 3.
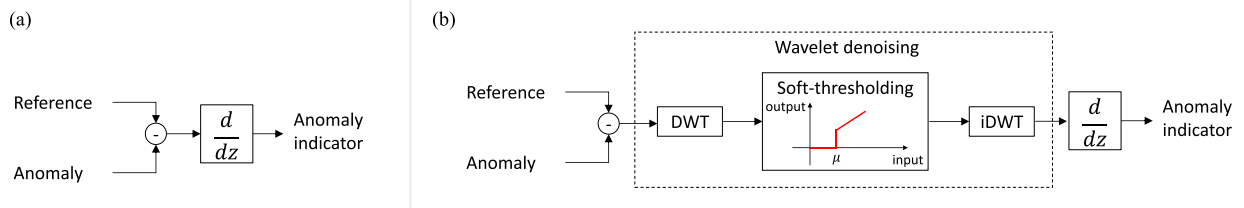

Fig. 6. Anomaly detection schemes based on (a) the subtraction + differentiation and (b) wavelet denoising.

signature, in the proximity of 220 km, shows a cascaded effect at the in-line EDFA 3, which is a direct consequence of the different input spectrum experienced by this amplifier. In other words, the first tilt profile (from in-line EDFA 2) provokes a tilt in the in-line EDFA 3. This demonstrates how effective the link tomography can be in determining wavelength-dependent disruptions in optical links.

F. Improvement of Fault Visualization

A major challenge that lies ahead of detection schemes is their location accuracy. Although the results obtained from the subtraction scheme (Fig. 5(a)) can already provide an approximate indication of the location of the fault, Fig. 5(b) reveals that the non-uniformity and sparsity of the signatures can hinder this identification of the problem. One alternative to improve the subtraction scheme is by inserting a numerical differentiation with respect to the spatial domain, as proposed in [9] and likewise illustrated in Fig. 6(a). Yet, this approach is still very dependent on multiple trace averaging to guarantee an accurate estimation. Therefore, in this last subsection we propose a novel detection method based on wavelet denoising of the link tomography [27].

The wavelet transformation was particularly chosen as it can be efficiently used to distinguish features in the data with different scales, thus preserving important signal features while removing noise [28]. Hence, in order to analyze behaviors with abrupt changes, such as an anomaly, this method gives a better representation of the localized position with respect to the other two previous approaches, i.e., subtraction and subtraction +

differentiation. The flow diagram for this anomaly indicator scheme is represented in Fig. 6(b). Here, the first step involves subtraction of the link tomography with anomaly from the reference link tomography (without anomaly), similarly to what is proposed in [8]. Then, the result of this subtraction undergoes a transformation employing the wavelet function before being forwarded to a thresholding procedure, where the threshold value is considered as the noise floor and the values below it are discarded (set to zero). After this, an inverse wavelet transform is applied to return the signal to the original composition. These steps are known as wavelet denoising for removal of the undesired noise within the signal. Finally, a spatial-differentiator block prepares the resultant data for anomaly detection.

The first sub-function of the wavelet denoising block is the discrete wavelet transformation (DWT). Shortly, this mathematical transformation is a window function of discrete samples that moves forward within a given sampling interval and is expressed by:

$$DWT\left(X\right) = \sum_{k=0}^{L-1} X\left(k\right) \cdot \psi\left(k - \omega\right), \quad (1)$$

where X represents the samples of the input data, k is the sample index, L is the length of this data, ω is the delay parameter and ψ is the discretized mother wavelet [28]. In our study, the DWT was applied on a wavelength-basis, i.e., $X(k)$ corresponds to the output of the subtractor for an individual wavelength. Consequently, L is the length of this vector, in this case, $L = N_{seg} + 1 = 281$. In the scope of this analysis, the
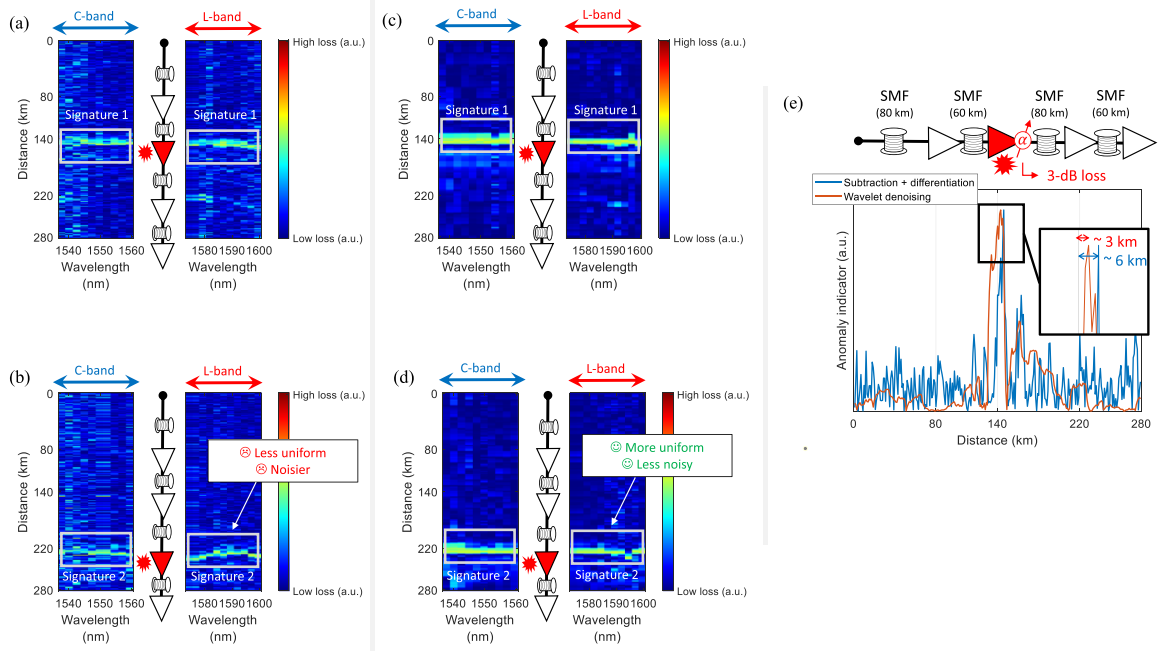
Fig. 7. Anomaly indication maps, when (a), (b) subtraction + differentiation and (c), (d) wavelet denoising are applied to detect power depletion in in-line EDFA 2 and in-line EDFA 3. (e) Anomaly detection curve for power depletion in in-line EDFA 2, when subtraction + differentiation and wavelet denoising are applied on a single wavelength (1549 nm). An accuracy improvement, by reduction of the location uncertainty in 3 km, can be achieved through wavelet denoising.

transformation was performed with the *sym4* wavelet function (mother wavelet) using the MATLAB© wavelet toolkit. Regarding the noise filtering, a universal threshold known as "Median" (μ) [29] was used for obtaining the threshold value:

$$\mu = \frac{\sqrt{2\log(N_{seg})\,\overline{X(k)}}}{0.6745}, \qquad (2)$$

where $\overline{\cdot}$ implies the mean value. With this, a soft thresholding [30] can be applied for filtering of the transformed data. The denoising step helps to minimize the secondary sharp variations in the anomaly indicator profile by thresholding the coefficients of the noisy components. Finally, an inverse DWT (iDWT) brings the signal that embodies the anomaly indicator back to its original domain.

In order to emulate anomalies that could affect the performance of the in-line EDFAs 2 and 3, an additional VOA was installed at the output of these amplifiers and programmed with a spectrally flat attenuation profile of 3 dB. We remind the reader that this a different scenario than the one evaluated in the previous subsection, where the attenuator was inserted at the input port the EDFA. This emulation of an anomaly, could, for example, correspond to an excessive loss originated from inappropriate amplifier-to-fiber connectors or simply a depletion in the amplifier's pump current.

Now, we investigate the application of the two anomaly detection methods depicted in Fig. 6(a), (b) to improve the visualization and location accuracy of the emulated faults on in-line EDFA 2 and 3. In Fig. 7(a), (b), it is possible to visualize on the heat map the result of the subtraction + differentiation method (Fig. 6(a)) for the in-line EDFA 2 and 3, respectively.

Qualitatively speaking, the heat maps can give a rough indication of the fault location, which in these two cases occurred in the vicinity of the 140th km (Fig. 7(a)) and 220th km (Fig. 7(d)). However, it is clearly visible that the "signature" caused by these anomalies leave a non-uniform pattern in the heat map, which is further penalized by the noisy profile of heat map. Now, in Fig. 7(c), (d), the outcome of the proposed approach in Fig. 6(b) is evaluated. In this new method, it is possible to observe that a significant improvement with respect to the noisy profile experienced in Fig. 7(a), (b) was achieved. Additionally, an enhancement regarding the uniformity of the signature is likewise possible in comparison to Fig. 7(a), (b).

Quantitatively, it is also possible to measure an improvement with respect to the location of the anomaly. In the plot in Fig. 7(e), we illustrate, for a fixed wavelength (1549 nm), the results from subtraction + differentiation and wavelet denoising to locate the positioning of the fault, i.e., position of in-line EDFA 2. As can be seen, the proposed approach, i.e., via wavelet denoising, can improve the location of the fault by 3 km, which in this case is represented by the position of peak in Fig. 7(e). Furthermore, a smoother anomaly detection curve (red solid line) is acquired, in comparison to the subtraction + differentiation method (blue solid line). This helps to easily distinguish the real anomaly from other irrelevant spikes that may lead to false conclusions.

V. CONCLUSION

In this work, we have experimentally investigated the application of Rx-DSP for gain estimation, power visualization and anomaly detection in C+L-band systems without directly using measurement devices.

After a brief introduction about the proposed link tomography, in Section III, the results of a single-channel experimental campaign were discussed. In that regard, we have shown with our investigations in Section IV that the extraction of spectral gain of in-line EDFAs from the terminal side is possible and can provide a sub-dB accuracy when compared to a b2b characterization carried out with an OSA.

In the sequence, we extended our analysis to study the application of the same scheme in more realistic transmission scenarios that account for the presence of co-propagating channels. In this case, we have shown how the link tomography reveals the natural evolution of the tilts along the link. Additionally, we have also proven that the proposed scheme is efficient in generating important visualizations in wavelength- and spatial-domain of events that can lead to unnatural gain tilts.

Finally, we propose a new failure detection scheme based on wavelet denoising that helps to improve the visualization of faults by delivering more uniform and less noisy readings of anomaly signatures.

We believe that relevant investigations for the future are: 1) the impact of the transceiver non-idealities on the accuracy of the link tomography; 2) application of the link tomography in heterogeneous multi-span links with densely loaded grid. With respect to 1), we expect that transceiver impairments (e.g., IQ imbalances, nonlinearities) can impact the accuracy of the approach. Therefore, an interesting study for the future is how susceptible the gain extraction or the anomaly detection are to transceiver-induced impairments. Concerning 2), we also foresee that in heterogeneous multi-span links, i.e., with diverse fiber types, the in-situ PPE needs improved mechanisms, given that, as of now, it assumes that fiber properties are constant across the link. Moreover, in densely packed grids the effect of the XPM may be so severe that it can hinder the SPM estimation, hence, in this scenario we believe that the longitudinal power estimation may require extra enhancements.

REFERENCES

[1] A. Ferrari et al., "Assessment on the achievable throughput of multi-band ITU-T G.652.D fiber transmission systems," *J. Lightw. Technol.*, vol. 38, no. 16, pp. 4279–4291, Aug. 2020.

[2] J. Renaudier et al., "107 Tb/s transmission of 103-nm bandwidth over 3×100 km SSMF using ultra-wideband hybrid Raman/SOA repeaters," presented at the *Opt. Fiber Commun. Conf. Exhib.*, 2019, Paper Tu3F.2.

[3] L. Rapp and M. Eiselt, "Optical amplifiers for wideband optical transmission systems," presented at the *Opt. Fiber Commun. Conf. Exhib.*, 2021, Paper Th4C.1.

[4] R. Kraemer et al., "Multi-band photonic integrated wavelength selective switch," *J. Lightw. Technol.*, vol. 39, no. 19, pp. 6023–6032, Oct. 2021.

[5] N. K. Fontaine, M. Mazur, R. Ryf, H. Chen, L. Dallachiesa, and D. T. Neilson, "36-THz bandwidth wavelength selective switch," presented at the *Eur. Conf. Opt. Commun.*, 2021, Paper PD2.3.

[6] C. Doerr et al., "O, E, S, C, and L band silicon photonics coherent modulator/receiver," presented at the *Opt. Fiber Commun. Conf. Exhib.*, 2016, Paper Th5C.4.

[7] T. Tanimura, S. Yoshida, K. Tajima, S. Oda, and T. Hoshida, "Concept and implementation study of advanced DSP-based fiber-longitudinal optical power profile monitoring toward optical network tomography [Invited]," *J. Opt. Commun. Netw. (JOCN)*, vol. 13, no. 10, pp. E132–E141, Oct. 2021.

[8] T. Tanimura, K. Tajima, S. Yoshida, S. Oda, and T. Hoshida, "Experimental demonstration of a coherent receiver that visualizes longitudinal signal power profile over multiple spans out of its incoming signal," presented at the *Eur. Conf. Opt. Commun.*, 2019, pp. 1–4.

[9] T. Tanimura, S. Yoshida, K. Tajima, S. Oda, and T. Hoshida, "Fiber-longitudinal anomaly position identification over multi-span transmission link out of receiver-end signals," *J. Lightw. Technol.*, vol. 38, no. 9, pp. 2726–2733, May 2020.

[10] T. Sasai, M. Nakamura, E. Yamazaki, S. Yamamoto, H. Nishizawa, and Y. Kisaka, "Digital longitudinal monitoring of optical fiber communication link," *J. Lightw. Technol.*, vol. 40, no. 8, pp. 2390–2408, Apr. 2022.

[11] T. Sasai, M. Nakamura, E. Yamazaki, and Y. Kisaka, "Precise longitudinal power monitoring over 2,080 km enabled by step size selection of split step Fourier method," presented at the *Opt. Fiber Commun. Conf. Exhib.*, 2022, Paper Th1C.4.

[12] T. Sasai, M. Nakamura, E. Yamazaki, S. Yamamoto, H. Nishizawa, and Y. Kisaka, "Digital backpropagation for optical path monitoring: Loss profile and passband narrowing estimation," presented at the *Eur. Conf. Opt. Commun.*, 2020, pp. 1–4.

[13] T. Sasai et al., "Simultaneous detection of anomaly points and fiber types in multi-span transmission links only by receiver-side digital signal processing," presented at the *Opt. Fiber Commun. Conf. Exhib.*, 2020, Paper Th1F.1.

[14] T. Sasai, M. Nakamura, T. Kobayashi, H. Kawakami, E. Yamazaki, and Y. Kisaka, "Revealing Raman-amplified power profile and Raman gain spectra with digital backpropagation," presented at the *Opt. Fiber Commun. Conf. Exhib.*, 2021, pp. 1–3.

[15] M. Eto, K. Tajima, S. Yoshida, S. Oda, and T. Hoshida, "Location-resolved PDL monitoring with Rx-side digital signal processing in multi-span optical transmission system," presented at the *Opt. Fiber Commun. Conf. Exhib.*, 2022, Paper Th1C.2.

[16] M. Sena, R. Emmerich, B. Shariati, J. K. Fischer, and R. Freund, "Link tomography for amplifier gain profile estimation and failure detection in C+L-band open line systems," presented at the *Opt. Fiber Commun. Conf. Exhib.*, 2022, Paper Th1H.1.

[17] M. Sena et al., "DSP-based link tomography for amplifier gain estimation and anomaly detection in C+L-band systems," *J. Lightw. Technol.*, vol. 40, no. 11, pp. 3395–3405, Jun. 2022.

[18] A. Turukhin et al., "Power-efficient transmission using optimized C+L EDFAs with 6.46 THz bandwidth and optimal spectral efficiency," presented at the *Eur. Conf. Opt. Commun.*, 2018, pp. 12–14.

[19] V. Lopez et al., "Optimized design and challenges for C&L band optical line systems," *J. Lightw. Technol.*, vol. 38, no. 5, pp. 1080–1091, Mar. 2020.

[20] H. D. Kim and C. H. Lee, "Capacities of WDM transmission systems and networks limited by stimulated Raman scattering," *IEEE Photon. Technol. Lett.*, vol. 13, no. 4, pp. 379–381, Apr. 2001.

[21] N. Deng, L. Zong, H. Jiang, Y. Duan, and K. Zhang, "Challenges and enabling technologies for multi-band WDM optical networks," *J. Lightw. Technol.*, vol. 40, no. 11, pp. 3385–3394, Jun. 2022.

[22] B. Correia et al., "Power control strategies and network performance assessment for C+L+S multiband optical transport," *J. Opt. Commun. Netw.*, vol. 13, no. 7, pp. 147–157, Jul. 2021.

[23] Y. Song, Q. Fan, D. Wang, C. Lu, A. Pak, and T. Lau, "A fast amplifier gain and tilt configuration algorithm for dynamic C+L-band networks," presented at the *Opt. Fiber Commun. Conf. Exhib.*, 2022, Paper Th1H.2.

[24] E. Ip and J. M. Kahn, "Compensation of dispersion and nonlinear impairments using digital backpropagation," *J. Lightw. Technol.*, vol. 26, no. 20, pp. 3416–3425, Oct. 2008.

[25] A. May, F. Boitier, E. Awwad, P. Ramantanis, M. Lonardi, and P. Ciblat, "Receiver-based experimental estimation of power losses in optical networks," in *IEEE Photon. Technol. Lett.*, vol. 33, no. 22, pp. 1238–1241, Nov. 2021.

[26] R. Emmerich et al., "Enabling S-C-L-band systems with standard C-band modulator and coherent receiver using coherent system identification and nonlinear predistortion," *J. Lightw. Technol.*, vol. 40, no. 5, pp. 1360–1368, Mar. 2022.

[27] J. Yu, S. Zhu, C. L. Gutterman, G. Zussman, and D. C. Kilper, "Machine-learning-based EDFA gain estimation [Invited]," *J. Opt. Commun. Netw.*, vol. 13, no. 4, pp. B83–B91, Apr. 2021.

[28] C. P. Dautov and M. S. Ozerdem, "Wavelet transform and signal denoising using wavelet method," presented at the *IEEE Signal Process. Commun. Appl. Conf.*, 2018, pp. 1–4.

[29] A. Ramadhan, F. Mahmood, and A. Elci, "Image denoising by median filter in wavelet domain," *Int. J. Multimedia Appl.*, vol. 9, no. 1, pp. 31–40, 2017.

[30] G. Luo and D. Zhang, "Wavelet denoising," in *Advanced Wavelet Theory and Their Applications in Engineering, Physics Technology*. London, U.K.: IntechOpen, 2012, pp. 59–80.